Available online at www.sciencedirect.com

Chemical Engineering Research and Design

journal homepage: www.elsevier.com/locate/cherd

Fabrication of calcium phosphates with controlled properties using a modular oscillatory flow reactor

Anabela Veiga[a,b,c], Filipa Castro[a,b,*], António Ferreira[a,b], Ana L. Oliveira[c,**], Fernando Rocha[a,b]

[a] Laboratory for Process Engineering, Environment, Biotechnology & Energy, Dep. of Chemical Engineering, Faculty of Engineering of Porto, R. Dr. Roberto Frias, 4200-465 Porto, Portugal

[b] ALiCE - Associate Laboratory in Chemical Engineering, Faculty of Engineering, University of Porto, Rua Dr. Roberto Frias, 4200-465 Porto, Portugal

[c] Universidade Católica Portuguesa, CBQF - Centro de Biotecnologia e Química Fina – Laboratório Associado, Escola Superior de Biotecnologia, Rua Diogo Botelho 1327, 4169-005 Porto, Portugal

ARTICLE INFO

Article history:
Received 28 January 2022
Received in revised form 12 April 2022
Accepted 25 April 2022
Available online 28 April 2022

Keywords:
Calcium phosphates
Continuous process
Nano and microcarriers
Oscillatory flow reactors
Precipitation

ABSTRACT

Several technologies and synthesis routes have been implemented to produce calcium phosphates (CaPs) with distinct characteristics for biomedical applications. However, produce CaPs in a controlled way still represents a challenge. Oscillatory flow reactors (OFRs) are a technology ready to deliver in terms of mixing intensification in multiphase systems. In particular, continuous processes in OFRs improve control over the reaction conditions and can be implemented at an industrial scale. The aim of this work was to study for the first time the influence of the oscillation amplitude (x_0: 4, 8 and 18 mm) and frequency (f: 1.9, 4 and 6 Hz) as well as residence time (τ: 3.3, 6.6 min) on the final CaP particles' physicochemical properties using a continuous precipitation process in a novel modular oscillatory flow plate reactor (MOFPR). Furthermore, other parameters such as the initial reagents concentration, initial Ca/P molar ratio (Ca/P = 1.67, 1.33) and temperature (T = 37, 54 °C) were also assessed. The synthesized particles and overall process were compared with particles obtained using the same methodology in conventional reactors, evidencing the potential of this technology to fabricate CaPs with tailored properties for potential application as nano or microcarriers for biomedical applications.

1. Introduction

The global tissue engineering (TE) market size was calculated at $ 9.9 billion in 2019 and is expected to witness an annual growth rate of over 14.2% from 2020 to 2027 (Research, 2020). This is the result of the increasing cases of chronic diseases and trauma injuries, which consequently leads to a market growth and to a need for the development of innovative solutions (Mishra et al., 2016).

Calcium phosphates (CaP) such as hydroxyapatite (HAp) and brushite have been extensively studied and applied for bone-related applications, owing to their biocompatibility, osteoconductivity, and osteotransductivity (Bohner et al.,

Abbreviations: CaPs, Calcium phosphates; Ca/P, Calcium/Phosphate molar ratio; f, frequency; HAp, hydroxyapatite; MOFPR, modular oscillatory flow plate reactor; Re, Reynolds number; SPCs, smooth periodic constrictions; TE, tissue engineering; x_o, amplitude; τ, residence time

* Corresponding author at: Laboratory for Process Engineering, Environment, Biotechnology & Energy, Dep. of Chemical Engineering, Faculty of Engineering of Porto, R. Dr. Roberto Frias, 4200-465 Porto, Portugal.

** Corresponding author.

E-mail addresses: filipaj@fe.up.pt (F. Castro), aloliveira@porto.ucp.pt (A.L. Oliveira).

https://doi.org/10.1016/j.cherd.2022.04.036

2013; FLUIDINOVA, 2021; Sangi Co, 2021; Issa et al., 2022). In this context, micro and nano CaP particles can be applied for the development of pioneering biomaterials in TE approaches (Levingstone et al., 2019; Sokolova and Epple, 2021).

Among these, micro- and nano-carrier systems have emerged to promote high-yield culture of anchorage dependent cells providing appropriate microenvironments for cell interaction and growth in vitro (Martin et al., 2011; Sun et al., 2011). Moreover, these support matrices have been explored as carriers in the field of targeted drug delivery due to their potential to encapsulate various biologically active molecules (Pathak et al., 2019). However, synthesis of both micro- and nano-CaP particles still faces challenges that include the control of their physicochemical properties (e.g. chemical composition, surface topography and particle size), which are intrinsically related with the ability of the cells to populate them (Huang et al., 2019) and condition their efficiency of drug delivery (Sun et al., 2011; Zhaorigetu et al., 2003).

Although a variety of particles' shape are used as micro and nanocarriers (Wu et al., 2018; Liu et al., 2012), they can adopt the form of microspheres, to promote an homogeneous surface for cells attachment (Sun et al., 2011; Sart et al., 2013). However, this shape is challenging to sort or further process. In addition to being directly exposed to surrounding flows, the cells attached to spherical microcarriers are constantly changing location over time (Wu et al., 2018). Conventional methods to obtain microspheres include emulsification and polymerization, followed by additional treatments, hindering their continuous production and making the process too complex. Therefore, other anisotropic morphologies have been explored (Barzegari and Saei, 2012).

Precipitation is the most widely studied route to produce nano- and micro- CaP particles due to its low cost, simplicity and easy application in industrial production. It has been broadly used for the formation of CaPs with tailored properties, by controlling parameters such as the Ca/P molar ratio, temperature, pH and reaction time (Veiga et al., 2020; Veiga et al., 2020). CaP precipitation is usually carried out in stirred tank (ST) batch reactors that consist of an agitator and an integrated temperature control system (Castro et al., 2012) (Table 1). The main advantage of this type of reactor is its ease of implementation and low production costs (Gomes et al., 2008). However, its low mixing efficiency at the molecular level often leads to heterogeneous distributions of process parameters which can yield particles with a broad size distribution (Esposti et al., 2020) and affect chemical purity of the particles precipitated (Castro et al., 2014). This problem is intensified at larger scales (Veiga et al., 2020).

Oscillatory flow reactors (OFRs) operated in batch have been presented in the literature as an alternative to conventional stirred tank (ST) reactors owing to their effective mixing and enhanced mass and heat transfer. OFRs offer controlled and uniform mixing through an oscillatory flow mixing mechanism, which intensity can be tuned by the oscillation amplitude (x_o) and frequency (f) (McGlone et al., 2015). The oscillatory flow mixing acceleration is characterized by the formation of vortices, which are generated when the fluid interacts with the constrictions. This mechanism results in enhanced mixing within each inter-baffle cell (Cruz et al., 2019).

Despite its advantages, conventional OFR presents limitations associated with the existence of dead zones or stagnate regions near the angle between the baffles and the reactor. To overcome this problem Reis, (2006) proposed a mesoscale OFR with smooth periodic constrictions (SPCs) suitable for biotechnological processes, reducing shear stress that can be detrimental to bacterial and other cell culture (Reis, 2006). Moreover, SPCs allow better control over fluid convection and dispersion within the SPC tube through vortex rings detachment (Reis et al., 2004). When compared to ST batch reactors, OFRs with SPCs are reported to be more efficient in CaPs wet chemical precipitation, with HAp being synthetized 4 times faster and no intermediate CaP phases being obtained (Veiga et al., 2020) (Table 1).

Regarding the operation mode of OFRs, continuous processes allow a more efficient use of the reagents and a greater control over the operating parameters such as the temperature and the concentration of the reagents, thus allowing to obtain a more uniform product. Moreover, continuous production allows higher productivity to be achieved (Latocha et al., 2018). In the work of Castro et al., (2016) HAp with controlled properties was obtained in a scaled-up meso-OFR with SPCs operating in continuous mode, demonstrating the feasibility of this technology and its innovative potential (Table 1). However, problems associated with secondary nucleation, agglomeration, clogging and solid deposition have been reported (Cruz et al., 2019; Reis, 2006; Bianchi et al., 2020).

To overcome the current limitations of existing OFRs, a modular oscillator flow plate reactor (MOFPR) (WO/2017/175207) was developed by the Laboratory of Process Engineering, Environment, Biotechnology and Energy (LEPABE) (Ferreira et al., 2017). Its 2D-SPCs and rectangular cross-section enable reduced shear stress and improved solid suspension and transportation (Ferreira et al., 2017). Furthermore, the MOFPR technology is suitable for multiphase applications such as screening reactions, bioprocess, gas-liquid absorption, precipitation, and crystallization operating in batch or continuous mode (Cruz et al., 2019; Wang et al., 2017; Ferreira et al., 2014; McGlone et al., 2015).

In the present work, the development of fully characterized and controlled CaPs for TE was achieved for the first time through a continuous precipitation process in a MOFPR. To achieve the proposed goal 1) the influence of the oscillation x_o and f, residence time (τ), initial reagents concentration and Ca/P molar ratio, and temperature were firstly investigated; 2) afterwards, to present the MOFPR as a practical platform for TE, the potential applications of the different materials produced as carrier biomaterials was discussed in detail through the analysis of scientific papers where particles with similar characteristics have been successfully applied in this field.

2. Materials and methods

2.1. *Precipitation of calcium phosphates (CaPs)*

2.1.1. *Experimental set up*

The synthesis of CaP particles was carried out by a continuous precipitation process in a MOFPR made of Teflon with a transparent polycarbonate cover. As illustrated in Fig. 1, the experimental set-up consists in a reactor, provided with 2D smooth periodic constrictions (SPCs) that are present in two parallels faces of the rectangular cross section tube, and a mixing chamber (Festo). The MOFPR (75 mL) is jacketed to allow temperature control and connected to a thermostatic bath (Huber Ministat 125). The fluid was oscillated

Table 1 – Comparison of the outcomes of three CaP processing reactors, following the same synthesis methodology (temperature, initial concentration, initial Ca/P molar ratio) (Veiga et al., 2020; Veiga et al., 2020; Castro et al., 2013).

Reactor	Mode	Crystallinity	Productivity	Morphology	Volume	Temperature (°C)	Reagents	Residence time (min)	CaP phase	Mean particle size (μm)	Ca/P molar ratio	Final pH	Reaction time	Reference
Stirred tank 	Batch	Amorphous CaPs were obtained	Scale up meso-OFR > ST > meso-OFR	nano-sized rod particles	500 mL	37	$CaCl_2$.2 H_2O and Na_2HPO_4	–	HAp	0.070	1.68	≈ 6	2 h 30 min	(Veiga et al., 2020)
OFR with SPC (meso oscillatory flow reactor) 					4 mL					0.075	1.61		30 min	(Veiga et al., 2020)
Scale up meso-OFR 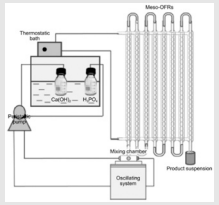	Continuous			Plate-shaped	≈ 32 mL (Eight meso-OFR)		$Ca(OH)_2$ and H_3PO_4	3.3–6.7 min		0.077	1.33		3 residence times (τ = 3.3 min)	(Castro et al., 2013)

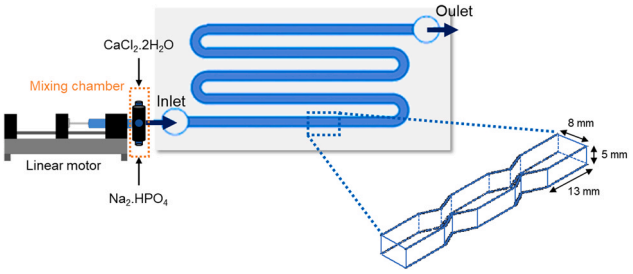

Fig. 1 – Experimental set-up for the continuous production of CaPs particles.

using a custom-build linear motor. A pH electrode (SenTix Mic-D, WTW) was placed at the exit of the MOFPR to measure the pH of the collected suspensions.

2.1.2. *Synthesis process*

CaP synthesis was carried out by mixing equal volumes of $CaCl_2.2\,H_2O$ (Merck, 99.5%) (pH=6) and Na_2HPO_4 (Sigma-Aldrich, 99.0%) (pH=9) solutions into a mixing chamber, using a peristaltic pump (Longer Pump, BT100–2J). Temperature inside the MOFPR was maintained by a thermostatic bath (Huber Ministat 125, connected to the MOFPR). Both calcium and phosphate solutions were prepared with ultrapure water (18.3 MΩ.cm^{-1} at 25 °C) and pre-heated prior being fed to the MOFPR (Elmasonic S 30 (H)).

Near-physiological conditions of pH and temperature based on a previous work (Veiga et al., 2021) were selected as starting point to produce HAp, and the effect of x_o, f, τ and Ca/P was assessed considering other works in which CaP were obtained in OFRs (Castro et al., 2014),(Castro et al., 2013). Higher concentrations of the initial precursor solutions were tested, to allow precipitation of other CaP phase, namely of brushite (Elliot, 1994). To evaluate the effect of temperature on the final properties of the particles synthetized, the maximum temperature allowed by the MOFPR was tested.

The flow conditions of the different experimental conditions studied in the MOFPR, can be characterized by the Reynolds Number (*Re*) and oscillatory Reynolds number (Re_0) (Table 2).

The *Re* describes the ratio of inertial forces to viscous forces in a flowing fluid (Eq. 1) and the Re_0 describes the intensity of mixing applied to the tube (Eq. 2) (Cruz et al., 2019):

$$Re = \frac{uD\rho}{\mu} \quad \text{Eq. 1}$$

where u is the superficial net flow velocity, D is the internal tube diameter in the straight section, ρ is the solution density, and μ is the solution viscosity.

$$Re_0 = \frac{2\pi f x_0 D\rho}{\mu} \quad \text{Eq. 2}$$

where f is the frequency of oscillation, and x_0 is the amplitude of oscillation (center-to-peak).

2.2. *Sample characterization*

For all the tested conditions, suspensions were collected after two residence times (6.6 min). This was done to guarantee that pH stabilization was achieved, which suggests that a stable CaP is formed (Elliot, 1994) (for conditions CaP1-CaP14 pH stabilized around 6 and for conditions CaP15-CaP16, it stabilized around 5).

2.3. *Phase identification*

The suspensions were collected at the MOFPR exit and filtered (0.2 µm pore size membrane, Gelman Sciences, USA). After washing with ultrapure water and ethanol, the particles were dried in the oven for 24 h at 80 °C. The obtained powders were used for Fourier-transform infrared spectroscopy (FTIR) (Bruker Vertex 70) and X-ray diffraction (XRD) (XPERT-PRO) analysis. The resulting supernatant from the filtration was used to determine the Ca/P molar ratio. Calcium concentration was determined by Atomic Absorption Spectrometry (λ = 422.7 nm, Flame: Air-acetylene, with addition of lanthanum) (Perkin Elmer AAnalyst 400) and phosphor concentration by UV-Vis Spectrophotometry - Molybdenum Blue (UV-Vis - Shimadzu UV –1800).

Table 2 – Experimental conditions for the precipitation of CaPs.

Sample	Initial concentration	Initial Ca/P molar ratio	Residence time (τ) (min)	Frequency (f) (Hz)	Amplitude (x_0) (mm)	T (°C)	Re_0	*Re*
CaP1	$CaCl_2.2\,H_2O$= 0.020 M; Na_2HPO_4 = 0.012 M	1.67	3.3	1.9	18.4	37	2222	96
CaP2		1.67	3.3	1.9	8.1	37	982.8	
CaP3		1.67	3.3	1.9	4.2	37	512.5	
CaP4		1.67	3.3	4	18.4	37	4678	
CaP5		1.67	3.3	4	8.1	37	2069	
CaP6		1.67	3.3	4	4.2	37	1079	
CaP7		1.67	3.3	6	18.4	37	7016	
CaP8		1.67	3.3	6	8.1	37	3103.5	
CaP9		1.67	3.3	6	4.2	37	1619	
CaP10		1.67	3.3	6	18.4	54	2222	
CaP11		1.67	3.3	6	8.1	54	982.8	
CaP12		1.67	3.3	6	4.2	54	512.5	
CaP13		1.33	3.3	1.9	4.2	37	512.5	
CaP14		1.67	6.6	1.9	4.2	37		48
CaP15	CaCl2.2H2O= 0.100 M; Na2HPO4 = 0.060 M	1.67	3.3	1.9	4.2	37		96
CaP16	$CaCl_2.2\,H_2O$= 0.200 M; Na2HPO4 = 0.120 M	1.67	3.3	1.9	4.24	37		

2.4. *Size and morphology*

For the particle size distribution by laser diffraction (LS 230, Beckman Coulter), the suspensions were directly analyzed without further treatment. Regarding scanning electron microscopy (SEM) (FEI Quanta 400FEG ESEM/EDAX Genesis X4M, amplified 10,000 times (1 μm) or 10,000 times (10 μm), beam intensity (HV) 25.00 Kv), the obtained powders were coated by a thin layer of gold prior the analysis.

3. Results and discussion

3.1. *Phase identification*

For the majority of the experimental conditions studied, the XRD patters were compared to a reference (JCPDS 00–009–0432) and to a commercial HAp (Spectrum, Calcium Hydroxyapatite, Powder, Minimum 40 Mesh) pattern indicating that the product formed is predominantly HAp-phase, exhibiting the typical hexagonal structure (Yang et al., 2013). Exceptions include CaP4-CaP6 (*f*=4 Hz), which in addition to presenting the characteristic peaks of HAp also match with brushite XRD pattern (Fig. 2A). Broadening and overlapping of the peaks is observed, namely at 26° 2θ and 30–34° 2θ,which may suggest that the particles obtained have low crystallinity and are at the nanoscale (Castro et al., 2013) (Supplementary information 1) (SI-1).

XRD patterns from the experimental conditions in which the initial reagents concentration was increased (CaP15 and CaP16) are similar to that of dicalcium phosphate dihydrate or brushite (DCPD) (RRUFF Database, ID: R070554.2). In Fig. 2B it is possible to detect the presence of peaks with high intensity at 11.6° 2θ, 20.7° 2θ, 29.14° 2θ, 31° 2 θ and 34° 2θ that corresponds to reported powder diffraction standards for

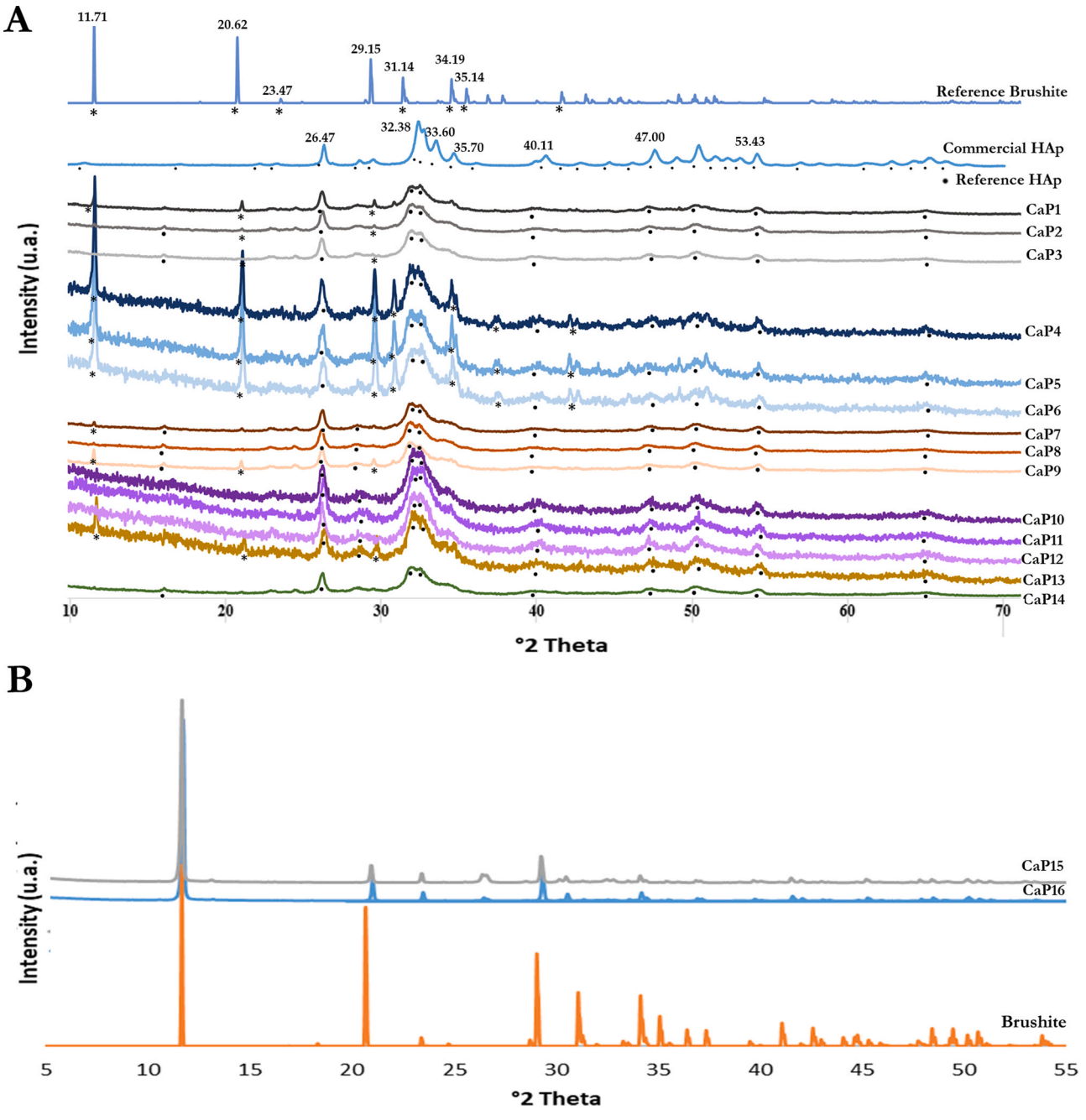

Fig. 2 – XRD patterns of the collected samples and of reference CaPs A) CaP1–14, B) CaP15, CaP16.

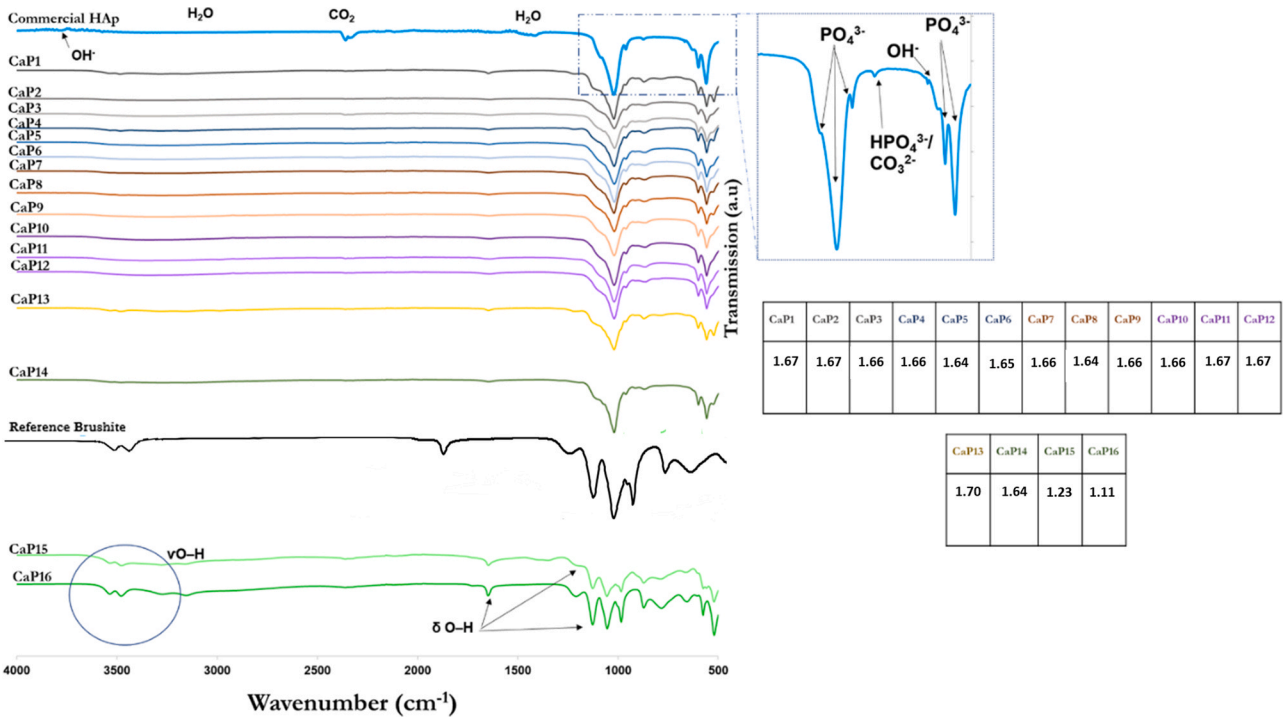

CaP1	CaP2	CaP3	CaP4	CaP5	CaP6	CaP7	CaP8	CaP9	CaP10	CaP11	CaP12
1.67	1.67	1.66	1.66	1.64	1.65	1.66	1.64	1.66	1.66	1.67	1.67

CaP13	CaP14	CaP15	CaP16
1.70	1.64	1.23	1.11

Fig. 3 – FTIR spectra of the collected samples, reference HAp and brushite, and Ca/P molar ratio of the samples collected.

crystalline brushite. The sharp peaks indicate that the samples have high crystallinity (Joint Committee for Powder Diffraction Standards JCPDS,) (SI-1).

The thermodynamically stable CaP phases can be consulted in phase diagrams that give an indication of the likely conditions required for synthesis (Mullin, 2002). However, the CaP phase that is formed is often dictated by kinetic considerations. According to the solubility isotherms for the system $Ca(OH)_2$-H_3PO_4-H_2O at normal temperatures and pressures, low concentrations promote the precipitation of HAp and minimize the precipitation of other CaP phases (Mullin, 2002). By increasing the initial concentration at the studied operating conditions (physiological conditions of temperature (37 °C) and pH (6–9)), brushite formation is faster than HAp, which explains the differences in the synthesized CaP phases (Elliot, 1994).

Based on peaks identified in FTIR spectra (Fig. 3), the synthetized products have a typical apatite structure, except for samples CaP15 and CaP16 which spectra are clearly distinct. Bands of ν_{3c} PO_4^{3-} stretching mode (around 1032 cm^{-1}), ν_1 PO_4^{3-} stretching mode (around 962 cm^{-1}) and ν_{4a} and ν_{4c} PO_4^{3-} bending mode (around 602 and 561 cm^{-1}) can be identified for the experimental conditions with low initial concentrations (CaP1-CaP14) (Koutsopoulos, 2002). Regarding OH^- peaks, it is difficult to identify ν_5 stretching mode (3572 cm^{-1}) as it can be overlapped by the band of adsorbed water (around 3700–3000 cm^{-1}). The absence of the peak assigned to ν_L vibrational mode (631 cm^{-1}) might be attributed to the substitution of OH^- ions by CO_3^{2-} ions, or to the substitution of PO_4^{3-} ions by CO_3^{2-} ions. According to Ren et al., (2014), where HAp was obtained by precipitation in aqueous system with an initial Ca/P molar ratio of 1.67, substitution of OH^- by CO_3^{2-} in the apatite lattice leads to a A-type carbonated apatite, and substitution of PO_4^{3-} by CO_3^{2-} leaving OH^- vacancy for charge compensation leads to a B-type carbonated apatite. This can explain the presence of a peak around 875 cm^{-1} that can be attributed to the bending mode of the CO_3^{2-} group, characteristic of carbonated apatites.

As regards to CaP15 and CaP16 samples, peaks assigned to brushite can be identified (Evan et al., 2005). The peaks around 3535 cm^{-1}, 3479 cm^{-1}, 3273 cm^{-1}, 3160 cm^{-1} can be attributed to OH^- stretching of water. H–O–H symmetric bending vibrations corresponds to the peak at 1645 cm^{-1}; PO_4 bond, P═O stretching vibrations to the peak at 1130 cm^{-1}; 790 cm^{-1} and 660 cm^{-1} to liberation; and 528 cm^{-1} to ν_4 bending vibrations of (H–O–) P═O bond acid phosphate (Koutsopoulos, 2002; Suryawanshi and Chaudhari, 2014; Singh et al., 2010).

FTIR analysis was corroborated by the determination of the Ca/P molar ratio for the different produced particles. Samples CaP1-CaP14 have a Ca/P close to stoichiometric HAp (Ca/P = 1.67). The molar ratio of the non-stoichiometric HAp can slightly vary from this value as a result of the incorporation of small amounts of anions and cations in its atomic structure (Mostafa, 2005). Ca/P < 1.67 is associated with calcium deficient HAp, while Ca/P > 1.67 is related to carbonated apatites (Elliot, 1994). Regarding samples CaP15 and CaP16, Ca/P molar ratio is close to the value reported for brushite (Ca/P = 1) (Habraken et al., 2016).

3.2. *Size, morphology and crystallinity*

From Fig. 4 it is possible to observe that the experimental conditions CaP15 and CaP16 (where the initial reagent concentrations were increased five and ten times, respectively) present a plate like morphology mostly formed by micro sized parallelogram shapes that are stacked in multiple layers. Comparable particles were obtained in the work of Toshima and co-authors (Toshima et al., 2014), were brushite with plate structure was synthetized for experiments with low initial pH. The final pH for CaP15 and CaP16 (5), was lower (~5) than that verified for the remaining experimental conditions (~6). This is an indication that the synthetized particles correspond to a different CaP phase. As to particle size distribution (Table 3), (Fig. 6), the mean particle size (in number) of the samples that correspond to brushite (d_{50} ~

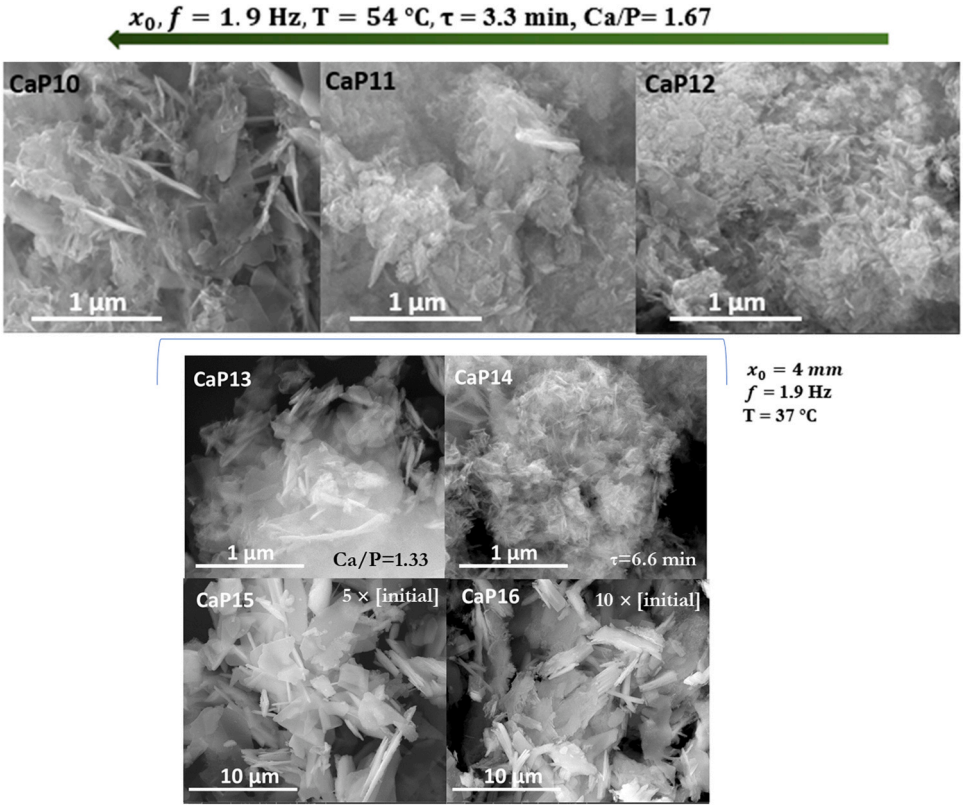

Fig. 4 – SEM images of the CaP10-CaP16 samples and particle size distributions in number. Scale bar CaP10-CaP14: 1 µm, CaP15-CaP16: 10 µm.

6 µm) are bigger than the other experimental conditions studied (d_{50} ~ 10 nm - 1 µm) (Figs. 4 and 5).

The initial Ca/P molar ratio was also associated with different morphologies. Compared to CaP3, CaP13 has more elongated particles (Fig. 4). These samples were obtained using the same experimental conditions of temperature, f, x_0, τ, only differing in the Ca/P molar ratio (1.67 and 1.33, respectively). Mixing molar ratio Ca/P = 1.33 has been employed in reported works, resulting in stable HAp nanoparticles suspensions with pH close to 7 (Castro et al., 2012; Castro et al., 2014; Castro et al., 2013; Castro et al., 2013).

On the other hand, it is possible to verify that the morphology of the particles formed is the same regardless τ (3.3 and 6.6 min for CaP3 and CaP14, respectively). Further, when analyzing the size distribution in number (Table 3), (Fig. 6) it seems that τ does not significantly influence the mean particle size (d_{50}) of the obtained HAp (Figs. 4 and 5). Esposti et al., (2020) studied the precipitation of calcium phosphate nanoparticles in a tubular reactor and found that particles dimensions are influenced by the reactor flow. Gecim et al., (2021) studied HAp precipitation in a continuous vortex reactor and in a semi-batch stirred tank and did not observe any significant influence of the reactant addition rate on particle size and morphology. In contrast to other reported works, the authors used diluted reactant solutions. They claim that the results obtained may be explained by the physical properties of the reactant solutions (low viscosity and low reactant concentration), providing higher mass diffusivities. According to McGlone et al., (2015), mixing is independent of the throughput velocity in oscillatory flow reactors. Therefore, it is possible to ensure good mixing through control of the oscillation conditions even at low net flow velocity, in contrast to conventional tubular reactors which rely on a high throughput velocity to achieve mixing.

Table 3 – Parameters of the particle size distribution in number and volume of the formed particles. d_{50}: 50% of the particles are smaller than this value; span: width of the distribution based on the 10%, 50% and 90% quantile.

Experimental condition	Number		Volume	
	d_{50} (µm)	span	d_{50} (µm)	span
CaP1	0.066	0.959	20.067	3.089
CaP2	1.021	1.411	15.489	1.549
CaP3	0.080	1.711	23.349	4.687
CaP4	0.089	1.942	15.381	11.291
CaP5	0.080	1.706	13.542	10.571
CaP6	0.083	1.842	14.548	11.465
CaP7	0.104	2.074	14.512	1.482
CaP8	0.069	1.402	19.166	2.357
CaP9	0.077	1.573	20.944	2.274
CaP10	4.435	1.362	12.977	15.632
CaP11	5.950	1.534	18.254	9.823
CaP12	0.075	1.447	15.094	11.067
CaP13	0.108	1.953	12.161	13.070
CaP14	0.076	1.543	23.776	2.549
CaP15	5.881	1.410	17.438	8.187
CaP16	6.398	1.410	18.267	7.894
Commercial HAp (Castro et al., 2013)	0.058	1.64	0.590	3.880

This may thus explain why we did not observe an influence of the reactant flow rate on particle morphology for the samples CaP3 and CaP14. The net flow rate was different (CaP3 – 22.72 mL/min; and CaP14 – 11.36 Ml/min), but the oscillatory flow conditions were the same for both samples. Further, low concentrated reactants solutions with low viscosity were used, providing thereby higher mass diffusivities. Moreover, through visual observations it was possible to verify that the number of particles formed is lower. In

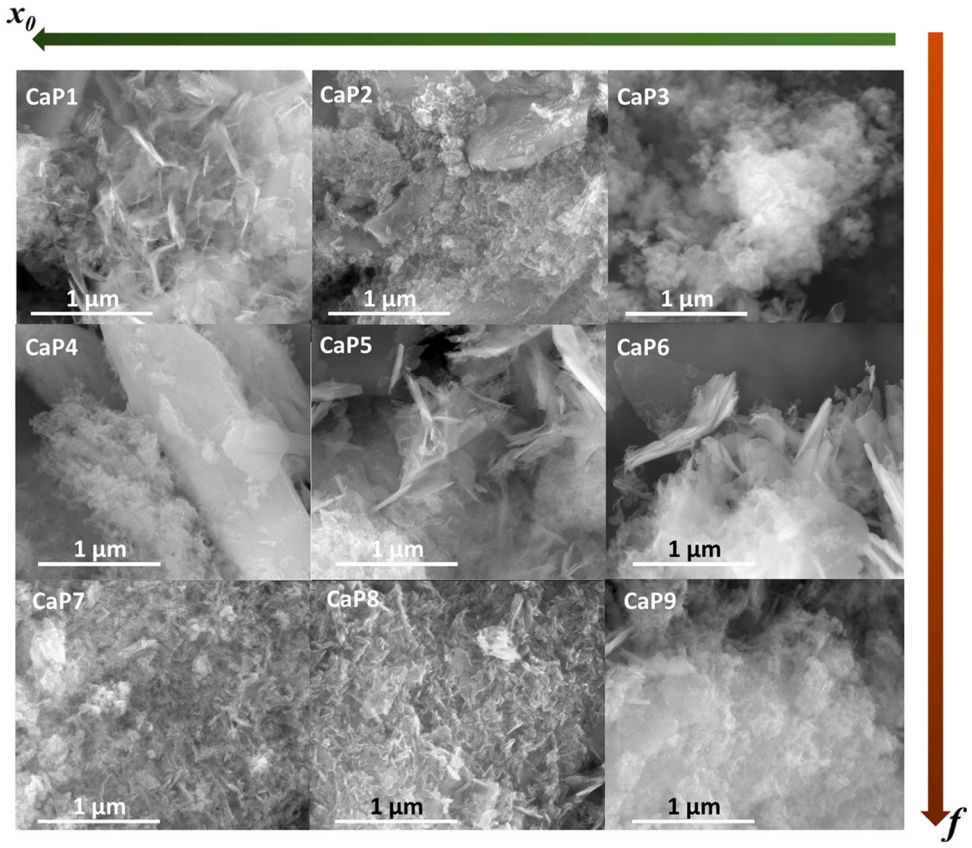

Fig. 5 – SEM images of the CaP1 to CaP9 samples.

fact, by quadrupling the τ (3.3 ×4 min), the amount produced was so small that it was not possible to characterize the sample using the techniques mentioned above. However, the suspension collected was used to perform laser diffraction, corroborating with the hypothesis that this factor does not affect the d_{50} (Fig. 6).

In CaP3 and CaP14, Re is 95.7 and 47.8, respectively, which is characteristic of a laminar flow (Re < 2300) (Reis, 2006; Mullin, 2002) Hence, decreasing fluid velocity and consequently Re can hinder the reaction yield. According to other works, mixing is more efficient for higher.

Re, providing more homogeneous reaction conditions and improving thus the monodispersity of synthesized particles (Castro et al., 2013; Günther and Jensen, 2006; Jähnisch et al., 2004). Moreover, by increasing the flow rate, more contact area between the reactant solutions is generated and thus micro mixing is improved. This leads to higher nucleation rates, explaining the higher amounts of precipitate obtained at shorter τ (Elliot, 1994; Mullin, 2002).

The remaining experimental conditions (CaP1-CaP12), corresponding to HAp predominantly at the nanoscale, take on a variety of morphologies with mean particle size (d_{50}) ranging from ~ 70 nm to 5 µm (Table 3) (Fig. 5). Although the particle size distribution in number of the samples CaP4 – CaP9 appear to be similar (Fig. 5), it is important to mention that particle size measurement by laser diffraction presents some limitations when particles with irregular shape (e.g., elongated, needle-shaped particles) are analyzed due to a spherical particle assumption (Grubbs et al., 2021). Thus, differences captured by SEM may not be detected in this technique. Further, nano particles, as mostly obtained in the present study, are prone to aggregation, as shown by the particle size distribution in volume (Table 3). Aggregates are very common in CaPs obtained in precipitation systems and result from the high surface-area-to-volume ratio of primary nanoparticles which, in order to reduce the high surface tension, adhere to one another (Castro et al., 2013; Mullin, 2002).

The conditions obtained with f = 4 Hz (CaP4, CaP5 and CaP6) clearly show the presence of micro scale plate-like structures surrounded by nano scale aggregated particles. The more crystalline microplates can correspond to brushite particles, which would explain the results obtained from XRD (Fig. 2) and which would imply the existence of a biphasic CaP system. The heterogeneous nature of these samples is evidenced by the distribution width (1.7 < span < 1.9), being especially high for x_0 = 18 mm (CaP4). As for f = 1.9 Hz (CaP1, CaP2 and CaP3), it was possible to obtain aggregated nanoparticles mainly composed by sharp structures for the highest amplitude (x_0 = 18 mm, CaP1) and rod-like particles with lower crystallinity for the smallest amplitude (x_0 = 4 mm, CaP3). The latter are similar to those obtained in previous works were low crystalline HAp was synthetized using a meso-OFR (Veiga et al., 2020).

For x_0 = 4 mm (CaP4-CaP6), in addition to rods, it is also possible to identify larger plates (d_{50} ~ 1 µm). The presence of different particle types is supported by the span > 1.7, which reflects the heterogeneous nature of these samples. Rod-like shaped nanoparticles were obtained in CaP7, CaP8 and CaP9 for 6 Hz. In the paper of Castro et al., (2016) identical HAp particles were obtained and reported to be 100 nm long and 20 nm width.

Thereby, the results suggest that for the lowest frequency (1.9 Hz), the effect of the amplitude (x_0) was more pronounced, having generated particles with more distinct characteristics in terms of size range and morphology. For higher f (4 and 6 Hz), x_0 does not seem to have a significant influence on the particles' final properties, being the

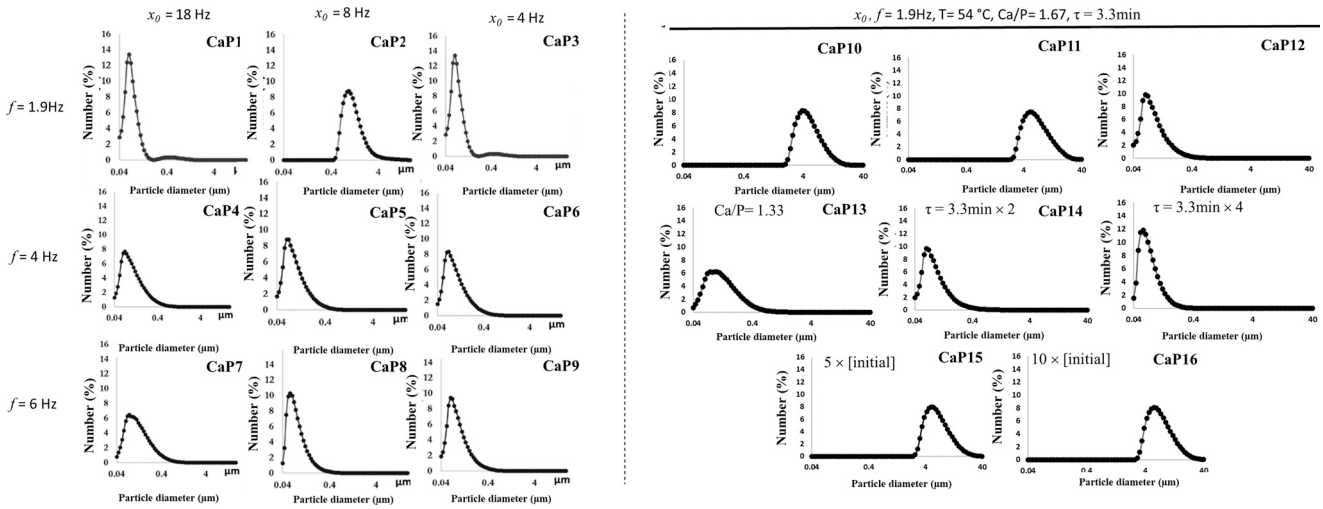

Fig. 6 – Particle size distribution in number for all the experimental conditions studied.

influence of f more pronounced. Cruz and co-authors (Cruz et al., 2019) suggested that increasing f up to 6 Hz in planar OFRs have a positive effect on the axial dispersion of solids, which may explain why for these experimental conditions (CaP7-CaP9) the particles have more homogeneous properties in terms of morphology and mean particle size in comparison with the conditions with lower frequencies (CaP1-CaP6) (Cruz et al., 2019). According to other studies (Reis et al., 2004; Smith and Mackley, 2006), f contributes essentially to increase the radial mixing which improves the generation and propagation of the vortices.

Micromixing has been shown to play a crucial role in precipitation processes since they involve fast chemical reactions (Elliot, 1994; Mullin, 2002; Mullin, 2001). Supersaturation, that determines nucleation and growth, is achieved when reactants are mixed and thus it is important to ensure effective micromixing when the reactants are added to enable homogeneous distribution of supersaturation and thereby the formation of particles with uniform characteristics. However, the processes following the mixing of the reagents also contribute to the final product properties. The CaPs precipitation system is usually characterized by the formation of intermediate CaPs phases (Castro et al., 2012; Veiga et al., 2020) that undergo phase transformation until the most stable CaP is formed. Ensuring good mixing is thus fundamental both at the location where the reactants are mixed but also in the rest of the experimental set-up constituted by the MOFPR itself. Avile and co-authors (Avila et al., 2018) studied the effect of the oscillatory conditions in the Nitech® continuous oscillatory baffled reactor for $Re_0 < 2000$ and demonstrated that x_0 and f contribute to micromixing even when reactants are added in a T junction before entering the reactor. Further, it is important to mention that even if micromixing can be the limiting step in precipitation processes, both micromixing and macromixing contribute to the final particles' characteristics. Judat et al., (Judat et al., 2004), verified the influence of micromixing intensity on the particle size and of macromixing on the particle morphology in precipitation experiments with barium sulfate. This is in agreement with the results of the present work, in which the influence of the oscillatory flow mixing on the final morphology of the particles manufactured is well evidenced.

Regarding the effect of temperature on the final characteristics of the CaP, an increase from 37 °C to 54 °C was associated with the formation of HAp with different particle mean size (d_{50}) and morphology (Fig. 4). Increasing temperature in HAp precipitation systems usually result in a crystal size increase (Lazić et al., 2001), which is in agreement with the presence of plates at the micro scale for both x_o = 18 (CaP10) and 8 mm (CaP11) experimental conditions. However, for x_0 = 4 mm (CaP12) the plates are smaller. Lee and co-authors reported that with increasing reaction temperature, the shape of the synthesized HAp particles changed from rod to leaf-like, which is in line with the finding of the present work (Lee et al., 2020).

3.3. *Comparison with other reactors used to produce CaPs*

HAp has been produced using mild conditions in terms of temperature, pH and reagents initial concentrations, by different reactor technologies (Veiga et al., 2020; Veiga et al., 2020; Castro et al., 2016) (Table 1). Although hydrodynamic conditions in the reactors are different and thus direct comparison is not possible, interesting observations can be done regarding each reactor performance in terms of reaction time and CaP particles characteristics.

In conventional ST, it was shown that when working at physiological conditions of temperature and pH, the precipitation process is characterized by the existence of three different stages, in which intermediate and less stable phases of CaP are formed before obtaining the most stable phase (HAp) (Castro et al., 2012). Therefore, although predominantly HAp-phase HAp is synthetized, the low mixing efficiency makes this process time consuming (≈ 2h30). As previously explained, mixing conditions play a key role in the characteristics of the particles resulting from a precipitation process, since precipitation is characterized by high supersaturations and very fast chemical reactions and nucleation kinetics. Even in stirred tanks reactors operated in semi-batch or continuous mode, macromixing is achieved by intensive stirring, but the micromixing is not at all controlled (Silva et al., 2008).

OFRs with SPC in batch have been presented in the literature as an alternative to conventional ST reactors owing their mixing efficiency and their enhanced heat and mass transfer (Mullin, 2002). Castro et al., (2014) compared the

Table 4 – Potential applications of the different CaPs produced.

CaP characteristics	Operation conditions using the MOFPR	Sample designation	Potential applications	Reference
Nano-HAp with rod-like morphology and low crystallinity.	- T = 37 °C, f= 1.9 Hz, x_0= 4 mm, Ca/P = 1.64, τ = 3.3 min CaP3	CaP3, CaP12, CaP14	Oral care products	(Coelho et al., 2019; Memarpour et al., 2019)
	- T = 54 °C, f= 6 Hz, x_0= 6 mm, Ca/P = 1.64 τ = 3.3 min		Injectable bone graft substitute	(Ryabenkova et al., 2017)
	- T = 37 °C, f= 1.9 Hz, x_0= 4 mm, Ca/P = 1.64, τ = 6.6 min		Coating material for bone-TE	(Wang et al., 2019)
			Drug delivery systems	(Mondal et al., 2018)
			Axonal guidance growth	(Liu et al., 2012)
			Wound healing	(Okabayashi et al., 2009)
Nano-HAp with rod-like elongated and low crystallinity.	- T = 37 °C, f= 1.9 Hz, x_0= 4 mm, Ca/P = 1.33, τ = 3.3 min	CaP13	Deliver media and scaffolds	(ZHANG and GONSALVES, 1997)
			Orthopedic implants	(D'Elía et al., 2015)
Nano-HAp with plate-like morphology and low crystallinity	- T = 37 °C, f= 6 Hz, Ca/P = 1.64, τ = 3.3 min	CaP1, CaP7, CaP8, CaP9	Mimicking the natural inorganic phase of bone	(Molino et al., 2020)
	- T = 37 °C, f= 1.9 Hz, x_0= 18 mm, Ca/P = 1.64, τ = 3.3 min		Cements for bone filling	(Espanol et al., 2010)
Plate/rod nano-HAp	- T = 37 °C, f= 4 Hz, Ca/P = 1.64, τ = 3.3 min	CaP2, CaP4, CaP5, CaP6	Induce apoptosis through changing mitochondrial membrane potential	(Xiong et al., 2016)
	- T = 37 °C, f= 1.9 Hz, x_0= 8 mm, Ca/P = 1.64, τ = 3.3 min			
Micro plate-like HAp	T = 54 °C, f= 6 Hz, x_0= 8, 18 mm, Ca/P = 1.64, τ = 3.3 min	CaP10, CaP11	Dental resin composite	(Zhao et al., 2019)
			Ceramic composites with load bearing applications for bone-TE	(Shen et al., 2001)
			Bio-filler for scaffold development	(Deb et al., 2019)
Plate-like brushite with high crystallinity.	T = 37 °C, f= 6 Hz, x_0= 4 mm, Ca/P = 1.64, τ = 3.3 min five or ten times the initial reagent concentration	CaP15, CaP16	Cement to repair bone defects	(Wen et al., 2009; Hirsch et al., 2014)
			Gene delivery applications	(Kumta et al., 2005)

performance of a ST (1 L) and a meso OFR (~4 mL) for the precipitation of HAp. The experiments were conducted at the same power density and results evidence the higher efficiency of the meso OFR over the ST, since HAp was synthetized about 4 times (≈30 min) faster and no intermediate CaP phases were obtained. However, the collected sample amount is reduced (Castro et al., 2014; Veiga et al., 2020). This type of system can be useful for preliminary studies and process optimization, reducing reagent requirements and waste and allowing to identify the most relevant reaction parameters (Castro et al., 2014; Veiga et al., 2020).

In the work of Castro et al., (2016), an experimental set up with scaled-up OFR was presented to continuously produce HAp with controlled properties. Although this process allows better control of mixing conditions and to obtain larger amounts of particles, OFR can be difficult to clean and lead to the deposition of precipitate on the reactor's walls (Reis, 2006; Ferreira et al., 2017).

In the present work, a MOFPR was used to overcome the limitations associated with solid handling such as solid deposition and fouling (Cruz et al., 2019; Lian et al., 2021). Indeed, no solid deposition neither fouling was observed during the experiments. The low reactants concentration, implying low amounts of precipitate, the short residence times and the oscillation conditions employed may have contributed to prevent solid deposition. Furthermore, the apparatus can be assembled and disassembled easily for cleaning (Ferreira et al., 2017). Moreover, stable particles were obtained only after 6.6 min. In this way, the high mixing efficiency and improved solid suspension and transportation as well as easy scale-up makes the MOFPR a promising technology for the production of CaP particles with tuned characteristics.

3.4. *Potential of the produced CaPs for biomedical applications*

The different properties of the manufactured CaPs, achieved by controlling the operating parameters, can be used for distinct applications in biomedical engineering. In addition to the possibility of scaling up the presented process, the quality of the CaP obtained in terms of batch-to-batch variability is a critical factor for the development of materials for TE. Thus, this work is a fundamental and preliminary step for the development of new biomaterials, with specific and reproducible properties.

Nano-rod and rod/plate and plate-like HAp with low crystallinity produced through a continuous process and in batch in other works (Veiga et al., 2020; Veiga et al., 2020; Castro et al., 2016) present similar physicochemical characteristics to the ones obtained in the present work (CaP1-CaP3, CaP7-CaP9, CaP12, CaP14). These particles have shown to stimulate cell proliferation of human osteoblastic-like (Saos-2) and induced better cell viability of human primary cells (HNDFs) when compared to a commercially available HAp (Veiga et al., 2020; Castro et al., 2016).

On the other hand, brushite with high crystallinity is widely used as a cement to repair bone defects, having a high resorption and new bone formation rate (Wen et al., 2009; Hirsch et al., 2014). Kumta et al., (2005), reported that the most challenging task of brushite materials was assuring the stability of this CaP, known to be a precursor for HAp formation. In our work, it was possible to control the stability of brushite particles, thus making the MOFPR a useful platform to produce brushite for biomedical applications (Table 4).

4. Conclusions

Calcium phosphates (CaPs) precipitation in conventional stirred tank (ST) batch reactors has disadvantages related with low mixing efficiency, product quality, process reproducibility and scale up. To overcome these limitations, modular oscillatory flow plate reactors (MOFPR) operated through a continuous process allow a more efficient control of the operational parameters in multiphase systems, especially when solids are involved. In addition, these reactors can be easily scaled-up and used at an industrial scale.

In this study, two major goals were achieved: to report for the first time the influence of several parameters on the final physicochemical characteristics of CaPs using an efficient continuous precipitation route in a new MOFPR; and to present potential applications for the different materials produced through comparison with the best available literature evidence.

Our findings suggest that the physical properties, in particular the morphology, of the synthetized HAp can be governed by the oscillation f and x_o. For lower frequencies (1.9 Hz), different x_o (4, 8 and 18 mm) lead to the production of distinct nano particles with a sharper, elongated or even rod-like morphology. At higher f (4 and 6 Hz), the x_o does not seem to have a significant influence on the particle's morphology. Plate-like and nano HAp particles with traces of brushite were obtained at 4 Hz, while only HAp nanorods were identified at 6 Hz.

τ seems to affect the reaction yield but not the particle characteristics. The increase in temperature led to the formation of larger and plate-shaped particles at the highest amplitudes. Regarding the initial concentration of reagents, it was found that this leads to the formation of highly crystalline brushite and that changing Ca/P ratio from 1.67 to 1.33 generates more elongated and calcium-rich particles.

The unique properties of the synthetized CaPs using specific mixing conditions (f, x_0) and different experimental conditions (Ca/P initial concentration and ratio, temperature), provide a new window for the rational design of tailored CaP -nano and micro-carriers for specific biomedical applications. Hence, the MOFPR represents an attractive platform to meet the current industry demands for CaPs with different characteristics for biomaterials and TE.

Author's contribution

The manuscript was written through contributions of all authors. All authors have given approval to the final version of the manuscript.

Declaration of Competing Interest

The authors declare that they have no known competing financial interests or personal relationships that could have appeared to influence the work reported in this paper.

Acknowledgments

This work was financially supported by: National Funds through FCT (Foundation for Science and Technology) under

the project UIDB/50016/2020 of the Centre for Biotechnology and Fine Chemistry - CBQF; and by LA/P/0045/2020 (ALiCE), UIDB/00511/2020 and UIDP/00511/2020 (LEPABE), funded by National Funds through FCT/MCTES (PIDDAC). A. Veiga gratefully acknowledges doctoral scholarship [2020.08683. BD] from FCT.

Appendix A. Supporting information

Supplementary data associated with this article can be found in the online version at doi:10.1016/j.cherd.2022.04.036.

References

A. Ferreira, F. Rocha, J. Teixeira, A. Vicente., Apparatus for mixing improvement based on oscillatory flow reactors provided with smooth periodic constrictions. Int. Patent WO 2015/056156 A1., PCT/IB2014/065273, 2014.

A. Ferreira, F. Rocha, J. Teixeira, F. Castro, Modular oscillatory flow plate reactor (WO 2017/175207 A1), 2017.

Barzegari, A., Saei, A.A., 2012. An update to space biomedical research: tissue engineering in microgravity bioreactors. BioImpacts. 2, 23–32. https://doi.org/10.5681/bi.2012.003

Bianchi, P., Williams, J.D., Kappe, C.O., 2020. Oscillatory flow reactors for synthetic chemistry applications. J. Flow Chem 10, 475–490. https://doi.org/10.1007/s41981-020-00105-6

Bohner, M., Tadier, S., van Garderen, N., de Gasparo, A., Döbelin, N., Baroud, G., 2013. Synthesis of spherical calcium phosphate particles for dental and orthopedic applications. Biomatter 3, e25103. https://doi.org/10.4161/biom.25103

Castro, F., Ferreira, A., Rocha, F., Vicente, A., António Teixeira, J., 2012. Characterization of intermediate stages in the precipitation of hydroxyapatite at 37 °C. Chem. Eng. Sci. 77, 150–156. https://doi.org/10.1016/j.ces.2012.01.058

Castro, F., Ferreira, A., Rocha, F., Vicente, A., Teixeira, J.A., 2013. Continuous-flow precipitation of hydroxyapatite at 37 °C in a meso oscillatory flow reactor. AIChE J. 59, 4483–4493. https://doi.org/10.1002/aic.14193

Castro, F., Kuhn, S., Jensen, K., Ferreira, A., Rocha, F., Vicente, A., Teixeira, J.A., 2013. Process intensification and optimization for hydroxyapatite nanoparticles production. Chem. Eng. Sci. 100, 352–359. https://doi.org/10.1016/j.ces.2013.01.002

Castro, F., Kuhn, S., Jensen, K., Ferreira, A., Rocha, F., Vicente, A., Teixeira, J.A., 2013. Continuous-flow precipitation of hydroxyapatite in ultrasonic microsystems. Chem. Eng. J. 215–216, 979–987. https://doi.org/10.1016/j.cej.2012.11.014

Castro, F., Ferreira, A., Rocha, F., Vicente, A., Teixeira, J., 2014. Precipitation of hydroxyapatite at 37° C in a meso oscillatory flow reactor operated in batch at constant power density. AIChE J 7, 405–410. https://doi.org/10.1002/aic

Castro, F., Ribeiro, V.P., Ferreira, A., Oliveira, A.L., Reis, R.L., Teixeira, J.A., Rocha, F., 2016. Continuous-flow precipitation as a route to prepare highly controlled nanohydroxyapatite: in vitro mineralization and biological evaluation. Mater. Res. Express. 3, 075404. https://doi.org/10.1088/2053-1591/3/7/075404

Coelho, C.C., Grenho, L., Gomes, P.S., Quadros, P.A., Fernandes, M.H., 2019. Nano-hydroxyapatite in oral care cosmetics: characterization and cytotoxicity assessment. Sci. Rep. 9, 11050. https://doi.org/10.1038/s41598-019-47491-z

Cruz, P., Silva, C., Rocha, F., Ferreira, A., 2019. The axial dispersion of liquid solutions and solid suspensions in planar oscillatory flow crystallizers. AIChE J. 65. https://doi.org/10.1002/aic.16683

D'Elía, N.L., Mathieu, C., Hoemann, C.D., Laiuppa, J.A., Santillán, G.E., Messina, P.V., 2015. Bone-repair properties of biodegradable hydroxyapatite nano-rod superstructures. Nanoscale 7, 18751–18762. https://doi.org/10.1039/C5NR04850H

Deb, P., Barua, E., Das Lala, S., Deoghare, A.B., 2019. Synthesis of hydroxyapatite from Labeo rohita fish scale for biomedical application. Mater. Today Proc. 15, 277–283. https://doi.org/10.1016/j.matpr.2019.05.006

Elliot, J.C., 1994. Struture and Chemistry of the Apatites and Other Calcium Orthophosphates, First ed.,. Elsevier.

Espanol, M., Portillo, J., Manero, J.M., Ginebra, M.P., 2010. Investigation of the hydroxyapatite obtained as hydrolysis product of α-tricalcium phosphate by transmission electron microscopy. CrystEngComm 12, 3318–3326. https://doi.org/10.1039/c001754j

Esposti, L.D., Dotti, A., Adamiano, A., Fabbi, C., Quarta, E., Colombo, P., Catalucci, D., De Luca, C., Iafisco, M., 2020. Calcium phosphate nanoparticle precipitation by a continuous flow process: a design of an experiment approach. Crystals 10, 1–17. https://doi.org/10.3390/cryst10100953

Evan, A.P., Lingeman, J.E., Coe, F.L., Shao, Y., Parks, J.H., Bledsoe, S.B., Phillips, C.L., Bonsib, S., Worcester, E.M., Sommer, A.J., Kim, S.A.M.C., Tinmouth, W.W., Grynpas, M., 2005. Crystal-associated nephropathy in patients with brushite nephrolithiasis. Kidney Int. 67, 576–591. https://doi.org/10.1111/j.1523-1755.2005.67114.x

FLUIDINOVA, FLUIDINOVA HYDROXYAPATITE, (2021). ⟨https://www.fluidinova.com/⟩(Accessed 23 July, 2021).

Gecim, G., Dönmez, S., Erkoc, E., 2021. Calcium deficient hydroxyapatite by precipitation: continuous process by vortex reactor and semi-batch synthesis. Ceram. Int. 47, 1917–1928. https://doi.org/10.1016/j.ceramint.2020.09.020

Gomes, J.F., Granadeiro, C.C., Silva, M.A., Hoyos, M., Silva, R., Vieira, T., 2008. An investigation of the synthesis parameters of the reaction of hydroxyapatite precipitation in aqueous media. Int. J. Chem. React. Eng. 6, 1–15. https://doi.org/10.2202/1542-6580.1778

Grand View Research, Tissue Engineering Market Size, Industry Analysis Report, 2027, (2020). ⟨https://www.grandviewresearch.com/industry-analysis/tissue-engineering-and-regeneration-industry⟩ (Accessed 7 May, 2021).

Grubbs, J., Tsaknopoulos, K., Massar, C., Young, B., O'Connell, A., Walde, C., Birt, A., Siopis, M., Cote, D., 2021. Comparison of laser diffraction and image analysis techniques for particle size-shape characterization in additive manufacturing applications. Powder Technol 391, 20–33. https://doi.org/10.1016/j.powtec.2021.06.003

Günther, A., Jensen, K.F., 2006. Multiphase microfluidics: from flow characteristics to chemical and materials synthesis. Lab Chip 6, 1487–1503. https://doi.org/10.1039/B609851G

Habraken, W., Habibovic, P., Epple, M., Bohner, M., 2016. Calcium phosphates in biomedical applications: materials for the future? Mater. Today. 19, 69–87. https://doi.org/10.1016/j.mattod.2015.10.008

Hirsch, A., Azuri, I., Addadi, L., Weiner, S., Yang, K., Curtarolo, S., Kronik, L., 2014. Infrared absorption spectrum of brushite from first principles. Chem. Mater. 26, 2934–2942. https://doi.org/10.1021/cm500650t

Huang, D., He, B., Mi, P., 2019. Calcium phosphate nanocarriers for drug delivery to tumors: imaging, therapy and theranostics. Biomater. Sci. 7, 3942–3960. https://doi.org/10.1039/C9BM00831D

Issa, K., Alanazi, A., Aldhafeeri, K.A., Alamer, O., Alshaaer, M., 2022. Brushite: Synthesis, Properties, and Biomedical Applications, in: Cryst. [Working Title]. IntechOpenhttps://doi.org/10.5772/intechopen.102007

Jähnisch, K., Hessel, V., Löwe, H., Baerns, M., 2004. Chemistry in microstructured reactors. Angew. Chemie Int. Ed. 43, 406–446. https://doi.org/10.1002/anie.200300577

Joint Committee for Powder Diffraction Standards (JCPDS) Reference Card Number 009–0077, n.d.

Judat, B., Racina, A., Kind, M., 2004. Macro- and micromixing in a taylor-couette reactor with axial flow and their influence on the precipitation of barium sulfate. Chem. Eng. Technol. 27, 287–292. https://doi.org/10.1002/ceat.200401997

Koutsopoulos, S., 2002. Synthesis and characterization of hydroxyapatite crystals: a review study on the analytical methods. J. Biomed. Mater. Res. 62, 600–612. https://doi.org/10.1002/jbm.10280

Kumta, P.N., Sfeir, C., Lee, D.-H., Olton, D., Choi, D., 2005. Nanostructured calcium phosphates for biomedical applications: novel synthesis and characterization. Acta Biomater 1, 65–83. https://doi.org/10.1016/j.actbio.2004.09.008

L. Sangi Co., The APatite Company, 2021. (n.d.). ⟨https://www.sangi-co.com/en/company/apataite-company/index.html⟩ (accessed July 23, 2021).

Latocha, J., Wojasiński, M., Sobieszuk, P., Ciach, T., 2018. Synthesis of hydroxyapatite in a continuous reactor: a review. Chem. Process Eng. Inz. Chem. i Proces. 39, 281–293. https://doi.org/10.24425/122950

Lazić, S., Zec, S., Miljević, N., Milonjić, S., 2001. The effect of temperature on the properties of hydroxyapatite precipitated from calcium hydroxide and phosphoric acid. Thermochim. Acta. 374, 13–22. https://doi.org/10.1016/S0040-6031(01)00453-1

Lee, I.H., Lee, J.A., Lee, J.H., Heo, Y.W., Kim, J.J., 2020. Effects of pH and reaction temperature on hydroxyapatite powders synthesized by precipitation. J. Korean Ceram. Soc. 57, 56–64. https://doi.org/10.1007/s43207-019-00004-0

Levingstone, T.J., Herbaj, S., Dunne, N.J., 2019. Calcium phosphate nanoparticles for therapeutic applications in bone regeneration. Nanomaterials 1570. https://doi.org/10.3390/nano9111570

Lian, S., Hu, Z., Lan, Z., Wen, R., Ma, X., 2021. Optimal operation of an oscillatory flow crystallizer: coupling disturbance and stability. ACS Omega 6, 28912–28922. https://doi.org/10.1021/acsomega.1c03890

Liu, M., Zhou, G., Song, W., Li, P., Liu, H., Niu, X., Fan, Y., 2012. Effect of nano-hydroxyapatite on the axonal guidance growth of rat cortical neurons. Nanoscale 4, 3201–3207. https://doi.org/10.1039/c2nr30072a

Liu, Y., Tan, J., Thomas, A., Ou-Yang, D., Muzykantov, V.R., 2012. The shape of things to come: importance of design in nanotechnology for drug delivery. Ther. Deliv. 3, 181–194. https://doi.org/10.4155/tde.11.156

M. Avila, M. Poux, J. Aubin, C. Xuereb, D.F. Fletcher, Characterization of micromixing in a Continuous Oscillatory Baffled Reactor, 16 (2018) 2–5.

Martin, Y., Eldardiri, M., Lawrence-Watt, D.J., Sharpe, J.R., 2011. Microcarriers and their potential in tissue regeneration. Tissue Eng. Part B Rev 17, 71–80. https://doi.org/10.1089/ten.teb.2010.0559

McGlone, T., Briggs, N.E.B., Clark, C.A., Brown, C.J., Sefcik, J., Florence, A.J., 2015. Oscillatory flow reactors (OFRs) for continuous manufacturing and crystallization. Org. Process Res. Dev. 19, 1186–1202. https://doi.org/10.1021/acs.oprd.5b00225

McGlone, T., Briggs, N.E.B., Clark, C.A., Brown, C.J., Sefcik, J., Florence, A.J., 2015. Oscillatory flow reactors (OFRs) for continuous manufacturing and crystallization. Org. Process Res. Dev. 19, 1186–1202. https://doi.org/10.1021/acs.oprd.5b00225

Memarpour, M., Shafiei, F., Rafiee, A., Soltani, M., Dashti, M.H., 2019. Effect of hydroxyapatite nanoparticles on enamel remineralization and estimation of fissure sealant bond strength to remineralized tooth surfaces: an in vitro study. BMC Oral Health 19, 1–13. https://doi.org/10.1186/s12903-019-0785-6

Mishra, R., Bishop, T., Valerio, I.L., Fisher, J.P., Dean, D., 2016. The potential impact of bone tissue engineering in the clinic. Regen. Med. 11, 571–587. https://doi.org/10.2217/rme-2016-0042

Molino, G., Palmieri, M.C., Montalbano, G., Fiorilli, S., Vitale-Brovarone, C., 2020. Biomimetic and mesoporous nano-hydroxyapatite for bone tissue application: a short review. Biomed. Mater. 15, 022001. https://doi.org/10.1088/1748-605X/ab5f1a

Mondal, S., Dorozhkin, S.V., Pal, U., 2018. Recent progress on fabrication and drug delivery applications of nanostructured hydroxyapatite. WIREs Nanomedicine and Nanobiotechnology 10, 1–32. https://doi.org/10.1002/wnan.1504

Mostafa, N.Y., 2005. Characterization, thermal stability and sintering of hydroxyapatite powders prepared by different routes. Mater. Chem. Phys. 94, 333–341. https://doi.org/10.1016/j.matchemphys.2005.05.011

Mullin, J.W., 2001. Crystallization, Fourth ed.,. Reed Educational and professional publishing Ltd, Oxford.

Mullin, J.W., 2002. Crystallisation. Org. Process Res. Dev. 6, 201–202. https://doi.org/10.1021/op0101005

N.M. Reis, Novel Oscillatory Flow Reactors for Biotechnological Applications, PhD thesis at the School of Engineering of the University of Minho, 2006.

Okabayashi, R., Nakamura, M., Okabayashi, T., Tanaka, Y., Nagai, A., Yamashita, K., 2009. Efficacy of polarized hydroxyapatite and silk fibroin composite dressing gel on epidermal recovery from full-thickness skin wounds. J. Biomed. Mater. Res. Part B Appl. Biomater. 90 B 90, 641–646. https://doi.org/10.1002/jbm.b.31329

Pathak, C., Vaidya, F.U., Pandey, S.M., 2019. Mechanism for /stem. In: Appl. Target. Nano Drugs Deliv. Syst. Elsevier, pp. 35–67. https://doi.org/10.1016/B978-0-12-814029-1.00003-X

Reis, N., Vicente, A.A., Teixeira, J.A., Mackley, M.R., 2004. Residence times and mixing of a novel continuous oscillatory flow screening reactor. Chem. Eng. Sci. 59, 4967–4974. https://doi.org/10.1016/j.ces.2004.09.013

Ren, F., Ding, Y., Leng, Y., 2014. Infrared spectroscopic characterization of carbonated apatite: A combined experimental and computational study. J. Biomed. Mater. Res. Part A. 102, 496–505. https://doi.org/10.1002/jbm.a.34720

Ryabenkova, Y., Pinnock, A., Quadros, P.A., Goodchild, R.L., Möbus, G., Crawford, A., Hatton, P.V., Miller, C.A., 2017. The relationship between particle morphology and rheological properties in injectable nano-hydroxyapatite bone graft substitutes. Mater. Sci. Eng. C. 75, 1083–1090. https://doi.org/10.1016/j.msec.2017.02.170

Sart, S., Agathos, S.N., Li, Y., 2013. Engineering stem cell fate with biochemical and biomechanical properties of microcarriers. Biotechnol. Prog. 29, 1354–1366. https://doi.org/10.1002/btpr.1825

Shen, Z.J., Adolfsson, E., Nygren, M., Gao, L., Kawaoka, H., Niihara, K., 2001. Dense hydroxyapatite-zirconia ceramic composites with high strength for biological applications. Adv. Mater. 13, 214–216 doi:10.1002/1521-4095(200102)13:3 < 214::AID-ADMA214 > 3.0.CO;2-5.

Silva, V., Quadros, P., Laranjeira, P., Dias, M., Lopes, J., 2008. A novel continuous industrial process for producing hydroxyapatite nanoparticles. J. Dispers. Sci. Technol. 29, 542–547. https://doi.org/10.1080/01932690701728924

Singh, S., Singh, V., Aggarwal, S., Mandal, U., 2010. Synthesis of brushite nanoparticles at different temperatures. Chem. Pap. 64, 491–498. https://doi.org/10.2478/s11696-010-0032-8

Smith, K.B., Mackley, M.R., 2006. An experimental investigation into the scale-up of oscillatory flow mixing in baffled tubes. Chem. Eng. Res. Des. 84, 1001–1011. https://doi.org/10.1205/cherd.05054

Sokolova, V., Epple, M., 2021. Biological and medical applications of calcium phosphate nanoparticles. Chem. A Eur. J. 27, 7471–7488. https://doi.org/10.1002/chem.202005257

Sun, L.-Y., Lin, S.-Z., Li, Y.-S., Harn, H.-J., Chiou, T.-W., 2011. Functional cells cultured on microcarriers for use in regenerative medicine research. Cell Transplant 20, 49–62. https://doi.org/10.3727/096368910X532792

Suryawanshi, V.B., Chaudhari, R.T., 2014. Growth and characterization of agar gel grown brushite crystals. Indian J. Mater. Sci. 2014, 1–6. https://doi.org/10.1155/2014/189839

Toshima, T., Hamai, R., Tafu, M., Takemura, Y., Fujita, S., Chohji, T., Tanda, S., Li, S., Qin, G.W., 2014. Morphology control of brushite prepared by aqueous solution synthesis. J. Asian Ceram. Soc. 2, 52–56. https://doi.org/10.1016/j.jascer.2014.01.004

Veiga, A., Castro, F., Reis, C.C., Sousa, A., Oliveira, A.L., Rocha, F., 2020. Hydroxyapatite/sericin composites: a simple synthesis route under near-physiological conditions of temperature and pH and preliminary study of the effect of sericin on the biomineralization process. Mater. Sci. Eng. C. 108, 110400. https://doi.org/10.1016/j.msec.2019.110400

Veiga, A., Castro, F., Oliveira, A., Rocha, F., 2020. High efficient strategy for the production of hydroxyapatite/silk sericin nanocomposites. J. Chem. Technol. Biotechnol. 96. https://doi.org/10.1002/jctb.6532

Veiga, A., Castro, F., Reis, C.C., Sousa, A., Oliveira, A.L., Rocha, F., 2020. Hydroxyapatite/sericin composites: a simple synthesis route under near-physiological conditions of temperature and pH and preliminary study of the effect of sericin on the biomineralization process. Mater. Sci. Eng. C. 108, 110400. https://doi.org/10.1016/j.msec.2019.110400

Veiga, A., Castro, F., Rocha, F., Oliveira, A., 2020. Silk-based microcarriers: current developments and future perspectives. IET Nanobiotechnology 14, 645–653. https://doi.org/10.1049/iet-nbt.2020.0058

Veiga, A., Castro, F., Rocha, F., Oliveira, A.L., 2021. A simple and controlled method for the continuous production of calcium/sericin-based composites. 5th YOUNG Polym. Sci. Semin. ⟨http://www.ictp.csic.es/ICTP2/es/SEJIPOL2021⟩.

Wang, H., Mustaffar, A., Phan, A.N., Zivkovic, V., Reay, D., Law, R., Boodhoo, K., 2017. A review of process intensification applied to solids handling. Chem. Eng. Process. Process Intensif 118, 78–107. https://doi.org/10.1016/j.cep.2017.04.007

Wang, J., Wang, M., Chen, F., Wei, Y., Chen, X., Zhou, Y., Yang, X., Zhu, X., Tu, C., Zhang, X., 2019. Nano-Hydroxyapatite Coating Promotes Porous Calcium Phosphate Ceramic-Induced Osteogenesis Via BMP/Smad Signaling Pathway. Int. J. Nanomedicine. Volume 14, 7987–8000. https://doi.org/10.2147/IJN.S216182

Wen, C.Y., Qin, L., Lee, K.M., Chan, K.M., 2009. The use of brushite calcium phosphate cement for enhancement of bone-tendon integration in an anterior cruciate ligament reconstruction rabbit model. J. Biomed. Mater. Res. Part B Appl. Biomater. 89, 466–474. https://doi.org/10.1002/jbm.b.31236

Wu, C.-Y., Stoecklein, D., Kommajosula, A., Lin, J., Owsley, K., Ganapathysubramanian, B., Di Carlo, D., 2018. Shaped 3D microcarriers for adherent cell culture and analysis. Microsystems Nanoeng. 4, 21. https://doi.org/10.1038/s41378-018-0020-7

Xiong, H., Du, S., Ni, J., Zhou, J., Yao, J., 2016. Mitochondria and nuclei dual-targeted heterogeneous hydroxyapatite nanoparticles for enhancing therapeutic efficacy of doxorubicin. Biomaterials 94, 70–83. https://doi.org/10.1016/j.biomaterials.2016.04.004

Yang, W.H., Xi, X.F., Li, J.F., Cai, K.Y., 2013. Comparison of crystal structure between carbonated hydroxyapatite and natural bone apatite with theoretical calculation. Asian J. Chem. 25, 3673–3678. https://doi.org/10.14233/ajchem.2013.13709

ZHANG, S., GONSALVES, K.E., 1997. Preparation and characterization of thermally stable nanohydroxyapatite. J. Mater. Sci. Mater. Med. 8, 25–28. https://doi.org/10.1023/A:1018586128257

Zhao, S.N., Yang, D.L., Wang, D., Pu, Y., Le, Y., Wang, J.X., Chen, J.F., 2019. Design and efficient fabrication of micro-sized clusters of hydroxyapatite nanorods for dental resin composites. J. Mater. Sci. 54, 3878–3892. https://doi.org/10.1007/s10853-018-3125-3

Zhaorigetu, S., Yanaka, N., Sasaki, M., Watanabe, H., Kato, N., 2003. Inhibitory effects of silk protein, sericin on UVB-induced acute damage and tumor promotion by reducing oxidative stress in the skin of hairless mouse. J. Photochem. Photobiol. B Biol. 71, 11–17. https://doi.org/10.1016/S1011-1344(03)00092-7